Third and fifth order nonlinear susceptibilities in thin HfO$_2$ layers

DAVID ZUBER,[1,2,*] SVEN KLEINERT,[1,2] AYHAN TAJALLI,[1,2,3] MORTEN STEINECKE,[4] MARCO JUPÉ,[2,4] IHAR BABUSHKIN,[1,2,5] DETLEV RISTAU,[1,2,4] AND UWE MORGNER[1,2,4]

[1]*Leibniz University Hannover, Institute of Quantum Optics, Welfengarten 1, 30167 Hannover, Germany*
[2]*Cluster of Excellence PhoenixD (Photonics, Optics, and Engineering-Innovation Across Disciplines), 30167 Hannover, Germany*
[3]*Currently in Deutsches Elektronen-Synchrotron DESY, Notkestraße 85, 22607 Hamburg, Germany*
[4]*Laser Zentrum Hannover e.V., Hollerithallee 8, 30419 Hannover, Germany*
[5]*Max Born Institute, Max-Born-Straße 2a, 10117 Berlin, Germany*
[*]*zuber@iqo.uni-hannover.de*

Abstract: Third harmonic generation (THG) from dielectric layers is investigated. By forming a thin gradient of HfO$_2$ with continuously increasing thickness, we are able to study this process in detail. This technique allows us to elucidate the influence of the substrate and to quantify the layered materials third $\chi^{(3)}(3\omega\colon \omega, \omega, \omega)$ and even fifth order $\chi^{(5)}(3\omega\colon \omega, \omega, \omega, \omega, -\omega)$ nonlinear susceptibility at the fundamental wavelength of 1030 nm. This is to the best of our knowledge the first measurement of the fifth order nonlinear susceptibility in thin dielectric layers.

1. Introduction

Within the last decade, the studying of nonlinear effects in dielectric coatings has rapidly increased. Especially the observation of two-photon-absorption [1], the Kerr-effect [2,3] and third harmonic generation (THG) [4–6] in thin dielectric layers and layer structures has attracted more attention. While two-photon absorption and the Kerr-effect have mainly been considered as effects that disturb the functionality of dielectric optics, third harmonic generation in dielectric layers has shown potential for efficient frequency conversion. Simple structures of two periodically alternating materials [6,7], which are quasi phase-matching structures, as well as aperiodic structures [5,8,9] have been reported on during the last years. In the latter case, conversion efficiency to the TH of 1.8 % was achieved [9]. This high conversion efficiency from micrometer-thick structures was made possible by two factors: high optical intensities (hundreds of GW,cm^{-1}) accessible with modern Ti:Sapphire and Yb-based lasers, and computer-based optimization of layer structure. To design such special layer structures, the properties of the materials, especially the linear and nonlinear susceptibilities play a decisive role; for THG, the third order susceptibility $\chi^{(3)}$ is the key parameter for prediction and optimization [8]. And even more precise, also the $\chi^{(5)}(3\omega : \omega, \omega, \omega, \omega, -\omega)$ contributes due to the high optical intensities.

Due to this, it is of significant importance to determine the optical properties of the used materials as accurate as possible. To achieve this, different approaches can be used, such as four-wave-mixing [10,11], Z-Scan [12] or direct THG [13,14]. While four-wave-mixing requires a complex optical setup to control two optical input fields in space and time, techniques that do not directly rely on THG can measure different contributions to the nonlinear optical susceptibility, such as nuclear motion-induced Raman scattering, which is not relevant for THG [10]. To minimize such influences, we focus on a technique that directly relies on THG measurement. In this case, the $\chi^{(3)}$ of thin layers is often estimated either by comparison to a material with well

known $\chi^{(3)}$ [13] or by an absolute measurement of the third harmonic power and a comparison to numerical models [14]. However, both techniques might deliver erroneous results, as the nonlinear contribution of the much thicker substrate is usually not distinguishable but often disregarded as negligible and the measurement of the layer thickness is limited to a few percent in precision in the nanometer range [14,15]. The latter is problematic, as the TH from thin layers strongly depends on the thickness, mainly due to interference effects inside the sample. This problem is often solved by studying several samples of different thickness [15] or by studying films with varying thickness along the surface of the substrate [14,16]. Such gradient layers with systematically varying thickness are studied here in this work. As we will show, studying the thickness-dependent TH in a thickness range from 200 nm to 1500 nm enables us to precisely measure the third order nonlinear susceptibility $\chi^{(3)}$ of our HfO$_2$ layer at 1030 nm. In addition, we get insight into the influence of the substrate and other nonlinear effects on the THG caused by our fundamental pulse – in particular self-focusing in the substrate and fifth order effects in the layer.

Although values of $\chi^{(5)}$ in gases and solids have been obtained experimentally for several materials [17–24], most of these studies refer to the higher-order Kerr effect with $\chi^{(5)}(\omega : \omega, \omega, \omega, -\omega, -\omega)$, and in bulk geometries rather than in thin layers. Only in one recent case [25], nonlinear susceptibilities for the 7th, 9th, and 11th harmonic generated in 430 µm thick single crystalline sapphire wafers, were reported.

Our paper is, as we believe, the first measurement of the fifth order susceptibility $\chi^{(5)}$ for third-harmonic generation in thin solids.

2. Experimental setup

The samples used in this study are HfO$_2$ gradient layers produced at LZH (Laser Zentrum Hannover eV.) by ion beam sputtering (IBS) on 1 mm thick, rectangular UV-grade fused silica substrates [26,27]. To create the gradient, an aperture is placed between the Hf target and the substrate holder. The resulting layer thickness depends on the position of the substrate in the substrate holder. For this study, two samples are used with increasing thicknesses from 200 nm to 1100 nm and from 1100 nm to 1500 nm. The thickness of the layer is measured dependent on the position on the sample by a spectrophotometer (Lambda 19, Perkin Elmer) [28]. By measuring the transmission and reflectance of the sample spectrally resolved, the refractive index and the thickness can be estimated by the measured interference fringes [29]. The steepest gradient of the layer was found to be 860 nm cm^{-1}.

The experimental setup for the optical nonlinearity analysis of the samples is shown in Fig. 1. For the generation of the pump pulses the infrared spectral flank of a 80 MHz two-cycle titanium:sapphire laser [30] got filtered out and amplified in an Yb-based amplifier chain. First, an Yb:glass based fiber-amplifier (Valo Innovations / TEM Messtechnik) is used to decrease the repetition rate from 80 MHz to 2 MHz and boost the pulse energy from the pJ-range up to 400 nJ. Then, a home built Yb:YAG amplifier increases the energy further, resulting in sech^2-shaped, 730 fs (FWHM) pulses at 1030 nm with a pulse energy of up to 30 µJ [31]. The energy of the pulses can be controlled by a variable attenuator consisting of a half-wave plate and a thin-film polarizer. The energy range in the experiments was set to energies between 2 µJ and 5 µJ (corresponding to optical peak fluences for a Gaussian beam between 0.1 J cm^{-1} and 0.26 J cm^{-1}), as energies lower than 2 µJ lead to signals below the detection limit of the used photodiodes and energies higher than 5 µJ result in a destruction of the layers. The beam is then focused by a 100 mm focusing lens to a beam diameter of $w = 70$ µm (full width at $1/_e$ of maximum intensity), resulting a nearly Gaussian beam in the focus (shown in the inset of Fig. 1). The focusing geometry is chosen such that the confocal parameter is longer than the samples thickness, leading to a change in the beam size of less than 1 µm in the 1 mm thick sample, and an even smaller change inside the thin layer. Therefore, we can assume a constant beam size

within the sample. The beam is also small enough to assume a constant material thickness as well (assuming the steepest gradient of $860\,nm\,cm^{-1}$, the layer thickness is only changing by $6\,nm$ within the diameter of the beam). For the measurement, both samples of different thickness range are mounted side by side on a holder to ensure equal alignment. Scanning the samples along the gradient with a translation stage allows to record the thickness dependent third harmonic power. It is recollimated by an uncoated UV fused silica lens (Thorlabs, LA4380-ML) and separated from the fundamental beam by three subsequent dichroic mirrors (Thorlabs, HBSY13), which only reflect the third harmonic located around $343\,nm$ and transmit all other harmonics and the fundamental. The light is then measured by a UV-sensitive silicon carbide photodiode (ifw optronics, JEA2), which is not sensitive to the fundamental light. The diode is power-calibrated in-house by a separate UV-source with the same central wavelength. This together with the knowledge regarding the reflection and transmission behaviour of the optical elements in the setup, allows for a calibrated third harmonic power measurement. To get the conversion efficiency, the fundamental power is measured by a powermeter (Thorlabs, S415C) behind the focusing lens in front of the sample.
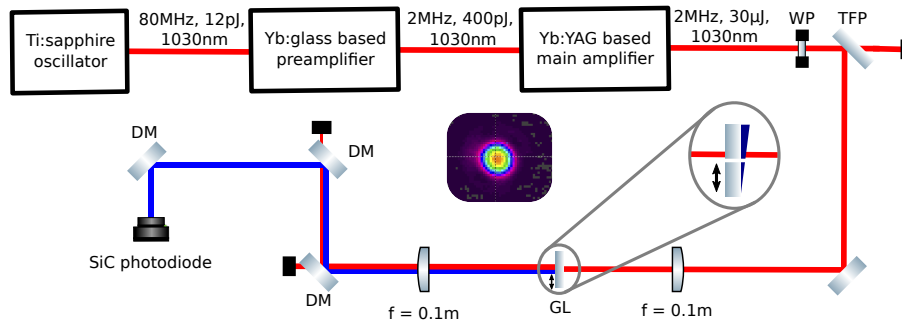

Fig. 1. Experimental setup. The seed pulse, generated by a Ti:sapphire oscillator is amplified in an Yb-based amplifier chain. The beam gets then attenuated to the desired pulse energy and focused onto the sample. The inset shows the beam profile in the focal plane. The generated TH is separated from the fundamental light and measured by a photodiode. WP: waveplate, TFP: thin-film polarizer, GL: gradient layer, DM: dichroic mirror, SiC photodiode: silicon carbide photodiode.

3. Numerical model

To extract the value of the nonlinear optical susceptibility and to elucidate the role of the layer and the substrate, numerical simulations based on a Finite Difference Time Domain (FDTD) method are performed [32], using the commercial software "Ansys Lumerical FDTD" [33], which allows to study linear and nonlinear effects in our structure. More precisely, the linear optical response and THG of the glass substrate as well as the dielectric layer are included in the model. The effects are impemented by the curl equations in nonmagnetic media issuing the atomic polarization

$$\vec{P} = \epsilon_0 \chi^{(1)} \vec{E} + \epsilon_0 \chi^{(3)} (3\omega | \omega, \omega, \omega) \vec{E}^3. \tag{1}$$

The electric field is derived from measured pulse parameters. In the time domain, the experimental pulse has a $sech^2$ shape, whereas a Gaussian pulse is used in the simulations. Furthermore, the plane wave in space used in the simulation is derived from the Gaussian beam in the experiments. These differences are taken into account by a correction factor of 1.065 when calculating the electric field strength. The frequency dependent $\chi^{(1)}$ of the substrate and the layer are taken from literature values [34,35], as well as the third order nonlinear susceptibility of

the substrate $\chi_S^{(3)}(3\omega|\omega,\omega,\omega)$ [36], leaving the third order nonlinear susceptibility of the layer $\chi_L^{(3)}(3\omega|\omega,\omega,\omega)$ as the only free parameter to fit the numerical results to the measured data. The thickness dependency is followed by changing the layer thickness from simulation to simulation.

In order to reduce computation time, the substrate thickness could be effectively reduced for the simulations: Since the TH from the substrate is oscillating periodically with changing material length l according to THG with phase mismatch ($\Delta k \neq 0$) [24], the substrate length can be reduced by even multiples of the coherence length $\pi/\Delta k$ without changing the expected THG. This assumption was tested by simulating the thickness dependent THG in the substrate. The results are shown in Fig. 2(a). Figure 2(b) shows the same simulations for the regions from 0 µm to 15 µm, 95 µm to 110 µm and 990 µm to 1010 µm performed with higher resolution. For substrate thicknesses below 100 µm, substrate surface interference effects start spoiling the layer effects. For thicker substrates, the finite bandwidth of the optical pulse will lead to slightly different coherence lengths of the different spectral components, resulting in reduced contrast between the maxima and minima of the oscillation. A chosen substrate thickness of around 100 µm forms a good compromise between small interference effects and an acceptable calculation time.
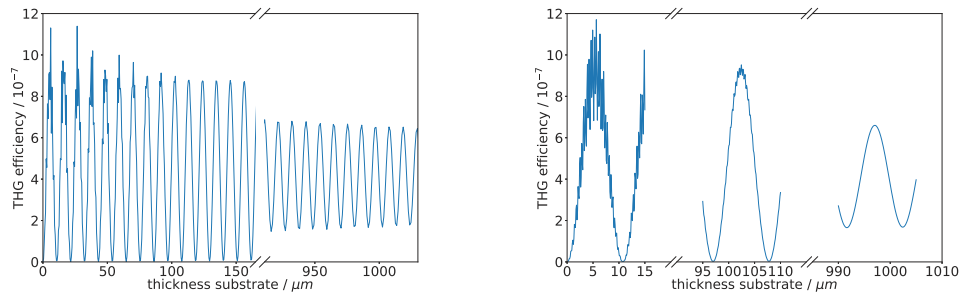

Fig. 2. Simulation of the expected TH from a substrate of changing thickness without any layer. (a) Comparison of the THG for substrate thicknesses from 0 µm to 150 µm and from 900 µm to 1100 µm. For lower thicknesses the influence of interference is visible. For thick substrates averaging effects caused by the non-monochromatic spectrum can be observed. (b) Detailed simulations for some regions from (a). The area around 100 µm shows a good compromise between the avoidance of interference effects and acceptable calculation time.

Based on the above considerations, two parameters have to be optimized to match the experimental results: $\chi_L^{(3)}$ and the exact substrate thickness (around 100 µm, modulo the coherence length). One parameter is scanned per simulation, while the other is kept constant. The results of the simulation have then been compared to the experimental result and, if necessary, one of both tuning parameters is changed again. These steps are repeated until agreement between the experimental and simulated data has been achieved.

4. Results and discussion

4.1. Influence of the substrate

In many previous studies, the influence of the substrate was declared negligible. This was either justified by the fact that the $\chi^{(3)}$ of the substrate is much smaller than that of the layer, or by the small confocal parameter of the driving beam and therefore low intensities in the substrate [14]. As both are not valid in our case, the substrate has been included into the simulations as a nonlinear material itself. As described in the previous section, this should lead to a thickness dependence of the TH not only from the layer, but also from the substrate. Fig. 3 shows the predicted TH yield for different layer and substrate thicknesses. The superimposed modulations of the TH due to interference in the layer and due to phase mismatch in the substrate are clearly distinguishable.

When the TH from the substrate is minimum, the net TH can be entirely attributed to the layer. By optimizing two parameters, the layers susceptibility $\chi_L^{(3)}$, and the substrate thickness (modulo its coherence length), the theoretical curve can be fitted to the experimental data. Figure 4 shows a comparison between the experimentally measured trace (blue, dotted, obtained with 5 µJ) and the simulated results (red, solid). The error bars are calculated from the input intensity and TH detection fluctuations (y-axis) and from the inaccuracy of the thickness measurement of the sample (x-axis). To increase the visibility, error bars are only shown for every twentieth measured data point. The third order nonlinear susceptibility of the substrate is taken from [36] as $\chi_S^{(3)} = 0.2 \times 10^{-21}$ m^2 V^{-2}. A good agreement between simulations and experiment is found for a substrate thickness of 105.5 µm (see white line in Fig. 3) and a layers third order nonlinear susceptibility of $\chi_L^{(3)} = 1.5 \times 10^{-21}$ m^2 V^{-2}. We also conducted numerical studies on the impact of the substrate's $\chi_S^{(3)}$ on the layer's $\chi_L^{(3)}$. Our findings show that changing the substrate's nonlinear susceptibility by 20 % requires a change in the layer's susceptibility of less than 1.5 % to compensate. As the change in the layer's susceptibility is negligible, we will assume the substrate's susceptibility value of $\chi_S^{(3)} = 0.2 \times 10^{-21}$ m^2, V^{-2} to be accurately precise for subsequent analyses.
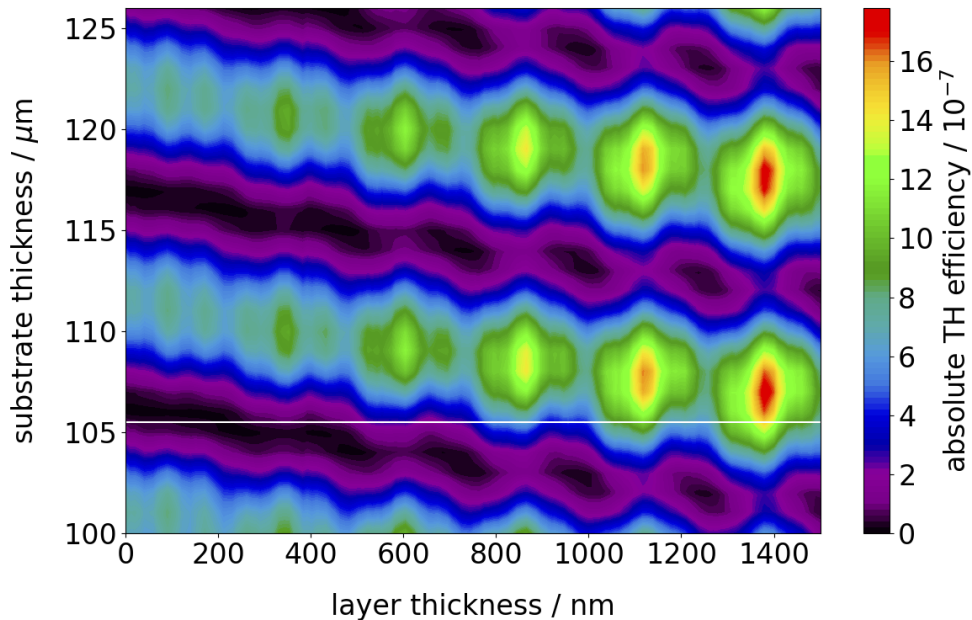

Fig. 3. Simulations showing the influence of the layers thickness and the substrates thickness on the absolute TH conversion efficiency. The white line corresponds to the simulated curve shown in Fig. 4.

The deviation between simulation and experiment in the layer thickness range below 500 nm is attributed to averaging effects caused by the finite bandwidth of the pulse in the substrate assumed thinner than it actually is.

It should be mentioned that an alternating approach to the use of gradient layers is to utilize a sample of fixed thickness and analyse the THG for different input angles. This technique suffers from three drawbacks, which are directly related to the presented results: First, realistically achievable thickness changes of the layer by a rotation of the sample are limited to a factor of 2. This might be not enough to study the THG over a complete coherence length. Second, the rotation of the sample will not only change the layers but also the substrate thickness. As shown
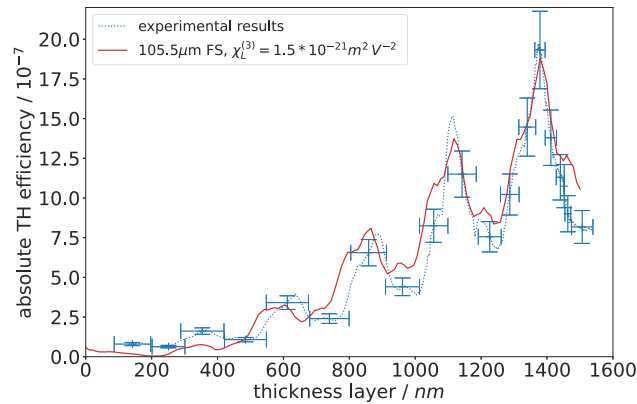
Fig. 4. Comparison of the experimentally (blue, dotted) and simulated (red, solid) absolute TH conversion efficiency after optimization of the substrates thickness and the layers $\chi_L^{(3)}$. The obtained value is $\chi_L^{(3)} = 1.5 \times 10^{-21}$ m^2 V^{-2}.

above, the substrate thickness needs to be precisely estimated within one coherence length in order to get correct results for the layers nonlinear susceptibility. In our approach this is possible, since the substrates thickness stays constant while the layers thickness is scanned. This leads to a redundancy of data, which helps to retrieve precise results for the layers nonlinear susceptibility. Third, the rotation of the sample will lead to a surface reflectivity change, which is furthermore dependent on the polarization and increases the complexity of the measurement further.

4.2. Estimation of the layer susceptibility $\chi_L^{(3)}$ and the influence of further nonlinear effects

For the experimentally obtained absolute TH conversion efficiency with 5 µJ of input pulse energy, simulations with a nonlinear susceptibility of $\chi_L^{(3)} = 1.5 \times 10^{-21}$ m^2 V^{-2} are found to agree well with the experimental data (see Fig. 4). Additional measurements are performed with different pulse energies and different orientations of the samples: substrate first or layer in front. Figure 5(a) shows the measured TH on a log-log plot with slopes of 3.96 and 4.00 if the beam passes the layer or the substrate first. These slope values indicate that other nonlinear effects contribute, as for pure TH a slope of 3 is expected. Taking into account the inclusion of other nonlinear effects, from now on we will call the retrieved susceptibility $\chi_{L, \text{eff}}^{(3)}$ until we are able to decouple the effects.

To check if the experimental data can be explained by THG only, simulations based on the FDTD approach presented in Chapter 3, are performed for each energy. If the yield can be explained by THG only, the experimental results should be reproducible with the same $\chi_{L, \text{eff}}^{(3)}$ for every energy. Figure 5(b) shows the results of these simulations and reveals two findings: First it can be observed that the required $\chi_{L, \text{eff}}^{(3)}$ is increasing with rising input energies (rising electric field amplitudes) for the substrate first (blue circles) and the layer first case (red squares). Second, it can be observed, that the substrate first case results in even higher $\chi_{L, \text{eff}}^{(3)}$ than the layer first case. Both effects give an indication that further nonlinear effects beside THG play a role in this measurement. The errors bars on the x-axis are given by the expected intensity fluctuations and measurement uncertainties obtained from the experiment. To obtain the error bars for the $\chi_{L, \text{eff}}^{(3)}$, the electric field strength in the simulations is changed by the amount corresponding to the fluctuations of the intensity measured in the experiment.
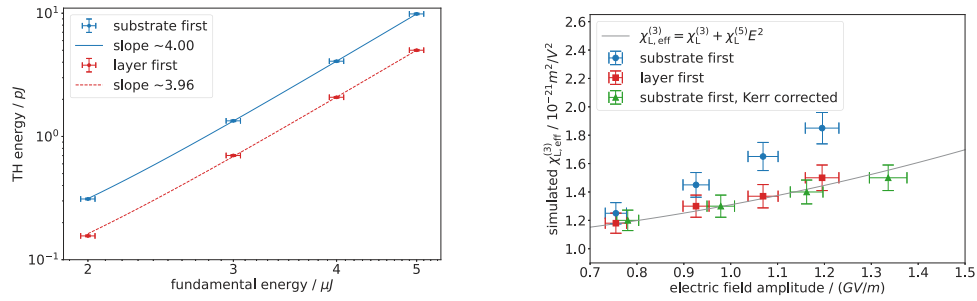
Fig. 5. (a) Dependency of the measured TH energy on the fundamental energy for the case of the substrate and the layer passed first. (b) $\chi^{(3)}_{L,\,eff}$ as function of the electric input field strength. The error bars on field axis are given by the energy fluctuations of the laser and the error of the $\chi^{(3)}_{L,\,eff}$ is estimated by simulations including the intensity fluctuations in the layer. The grey line represents a fit assuming contribution of fifth order effects.

4.2.1. Influence of the Kerr-effect

A possible explanation for the difference in the retrieved $\chi^{(3)}_{L,\,eff}$-values depending on the propagation direction can be the Kerr effect, more specifically self-focusing inside the substrate. Considering the case of passing the 1 mm thick substrate first before passing the HfO_2-layer, the beam size in the layer should be decreased if self-focusing is present, leading to an increase of the intensity inside the HfO_2-layer. As the TH is expected to be generated mostly in the HfO_2-layer, this change of intensity in the layer can explain the increased TH yield, resulting in higher $\chi^{(3)}_{L,\,eff}$-values in the simulation. Following the same argumentation, self-focusing should only play a minor role if the layer is passed first, resulting in a lower TH yield and smaller $\chi^{(3)}_{L,\,eff}$-values. An exact implementation of the Kerr-effect into our TH simulation is not possible, which is why we decided to simulate the self-focusing action independently by an ABCD-matrix based formalism [37] and correct the beam size inside the thin layer for the TH simulation accordingly. Note that any change in beam size within the sample is solely due to the substrate, as the self-focusing within the thin layer can be ignored due to its significantly smaller thickness.

This procedure leads to the following changes in the TH simulations: In the case where the substrate is passed first, the TH simulations are performed using the beam size that is given by the ABCD-calculations at the layers position. For the self-focusing calculations the nonlinear refractive index of quartz glass $n_2 = 2.2 \times^{-16}$ $cm^2\,W^{-1}$ [38] is used, leading to an increase of intensity inside the layer by 25 % for a pulse energy of 5 µJ. In the case where the layer is passed first, no change of the beam size is considered or expected. The result of the corresponding $\chi^{(3)}_{L,\,eff}$ retrievals is shown in Fig. 5(b). The $\chi^{(3)}_{L,\,eff}$ results for the Kerr-corrected, substrate-first case (green triangles) and layer first case match very well within each others error bars.

4.2.2. Influence of higher order effects

After ruling out the influence of the Kerr effect, there is still a clear trend towards increasing $\chi^{(3)}_{L,\,eff}$ for higher energies in Fig. 5(b). Further third order nonlinear effects such as self-phase modulation (SPM), self steepening (SST), or cross polarized wave generation (XPW) do not play any role. SPM, because the B-integral inside the sample is very small ($B<0.1\pi$), SST due to the long pulse duration [24], and XPW due to the layers isotropy [39]. Thermal effects could also be considered influencing the measurements [40] by layer absorption and thermal lensing. However due to the low absorption layer material and the small propagation length, it is negligible. There is also no indication for a thermal effects on the optical thickness of the layer, as all the maxima and minima are appearing at the same thickness for all measured energies (not shown here).

Finally, fifth order effects must be considered. Fifth harmonic generation will happen, but the setup is not sensitive for this wavelength range. Furthermore, fifth order effects contribute to the TH yield via

$$\chi_{\text{L, eff}}^{(3)} = \chi_{\text{L}}^{(3)} + \chi^{(5)}(3\omega|\omega,\omega,\omega,\omega,-\omega)E^2, \tag{2}$$

which is plotted as a grey line in Fig. 5. The retrieved third and fifth order nonlinear susceptibilities are

$$\chi_{\text{L}}^{(3)} = (1.0 \pm 0.17) \times 10^{-21} \text{ m}^2 \text{ V}^{-2} \text{ and} \tag{3}$$

$$\chi_{\text{L}}^{(5)} = (3.1 \pm 1.9) \times 10^{-40} \text{m}^4 \text{ V}^{-4}. \tag{4}$$

Comparable values for the third order nonlinear susceptibility of HfO_2 in the literature are obtained with 800 nm fundamental wavelength and are in a range of $0.9\times^{-21}$ $\text{m}^2 \text{ V}^{-2}$ to $4.2\times^{-21}$ $\text{m}^2 \text{ V}^{-2}$ [5,15], which is quite in line with our findings. Up to the authors knowledge, no study of $\chi^{(5)}(3\omega|\omega,\omega,\omega,\omega,-\omega)$ or other $\chi^{(5)}$ effects in HfO_2 have been reported yet. The ratio $\chi^{(3)}/\chi^{(5)}$ between the values reported in this study is in the order of 10^{-19}, which is similar to ratios of odd lower order nonlinear susceptibilities for other reported materials [18,19,25,36].

By comparing the third and fifth order nonlinear polarization terms, we can assume the contribution of $\chi^{(5)}(3\omega|\omega,\omega,\omega,\omega,-\omega)$ to the TH:

$$\frac{\chi^{(5)}E^5}{\chi^{(3)}E^3} \tag{5}$$

Using the electric field amplitudes, ranging from 7.803×10^8 V,m^{-1} to 1.336×10^9 V,m^{-1}, corresponding to the pulse parameters provided in the "experimental setup" section we can calculate the contribution of the fifth-order effect to TH, which ranges from 19 % to 55 %.

5.　Conclusion

In summary, we have studied low order nonlinear susceptibilities in a thin gradient HfO_2-layer. In comparison to studies with fixed layer thickness, the gradient layer approach allowed us to decouple the TH contribution of the substrate from the layers one. We have shown that in our case the nonlinearity of the substrate can not be neglected, as the values of the third order nonlinear susceptibility of the substrate and the layer are in the same order of magnitude. Further we were not only able to measure the third order nonlinear susceptibility of the layer with high accuracy, but also to analyze the contribution of other nonlinear effects, mainly the optical Kerr-effect and THG by fifth order nonlinearity. While the values obtained for the third order nonlinear susceptibility are in the range of previously measured values, the latter one represents, up the authors knowledge, the first measured value of fifth order nonlinearity by THG in dielectric materials and also the first measured value for the fifth order nonlinearity in thin HfO_2 films. The values for the nonlinear susceptibilities presented in this work show a similar ratio as nonlinear susceptibility values which have been presented in literature for different bulk materials. Thus we believe, that our method opens a way to measure nonlinear susceptibilities of different orders in thin dielectric layers with similar accuracy than in bulk materials. The results obtained here can also help to improve the understanding of more complex dielectric structures, such as THG-mirrors and might lead to a new generation of such mirror structures with high efficiencies.

Disclosures. The authors declare no conflicts of interest.

Data availability. Data underlying the results presented in this paper are not publicly available at this time but may be obtained from the authors upon reasonable request.

References

1. O. Razskazovskaya, T. T. Luu, M. Trubetskov, E. Goulielmakis, and V. Pervak, "Nonlinear absorbance in dielectric multilayers," Optica **2**(9), 803–811 (2015).
2. E. Fedulova, M. Trubetskov, T. Amotchkina, K. Fritsch, P. Baum, O. Pronin, and V. Pervak, "Kerr effect in multilayer dielectric coatings," Opt. Express **24**(19), 21802–21817 (2016).
3. T. Amotchkina, M. Trubetskov, and V. Pervak, "Experimental and numerical study of the nonlinear response of optical multilayers," Opt. Express **25**(11), 12675–12688 (2017).
4. T. Tsang, "Reflected optical harmonics from dielectric mirrors," Appl. Opt. **33**(33), 7720–7724 (1994).
5. C. Rodríguez, S. Günster, D. Ristau, and W. Rudolph, "Frequency tripling mirror," Opt. Express **23**(24), 31594–31601 (2015).
6. R. Biswas, M. Dandu, S. Menon, K. K. Jha, J. K. M. K. Majumdar, and V. Raghunathan, "Third-harmonic generation in multilayer Tin Diselenide under the influence of Fabry-Perot interference effects," Opt. Express **27**(20), 28855–28865 (2019).
7. O. Shramkova, "Loss-compensated active nonlinear layered structures with gain saturation," J. Opt. Soc. Am. B **36**(8), 2038–2044 (2019).
8. C. Rodríez and W. Rudolph, "Modeling third-harmonic generation from layered materials using nonlinear optical matrices," Opt. Express **22**(21), 25984–25992 (2014).
9. S. Balendat, M. Jupé, M. Steinecke, L. Jensen, A. K. Oskouei, W. Rudolph, D. Zuber, U. Morgner, and D. Ristau, "Manufacturing and characterization of frequency tripling mirrors," in *2021 Conference on Lasers and Electro-Optics Europe and European Quantum Electronics Conference (2021)*, (Optical Society of America, 2021), p. cd_p_33.
10. R. Hellwarth, J. Cherlow, and T.-T. Yang, "Origin and frequency dependence of nonlinear optical susceptibilities of glasses," Phys. Rev. B **11**(2), 964–967 (1975).
11. H. Q. Le, W. D. Goodhue, and K. Rauschenbach, "Measurement of third-order optical nonlinear susceptibility using four-wave mixing in a single-mode ridge waveguide," Opt. Lett. **15**(20), 1126–1128 (1990).
12. M. Sheik-bahae, A. A. Said, and E. W. V. Stryland, "High-sensitivity, single-beam n_2 measurements," Opt. Lett. **14**(17), 955–957 (1989).
13. R. Barille, L. Canioni, L. Sarger, and G. Rivoire, "Nonlinearity measurements of thin films by third-harmonic-generation microscopy," Phys. Rev. E **66**(6), 067602 (2002).
14. G. I. Petrov, V. Shcheslavskiy, V. V. Yakovlev, I. Ozerov, E. Chelnokov, and W. Marine, "Efficient third-harmonic generation in a thin nanocrystalline film of ZnO," Appl. Phys. Lett. **83**(19), 3993–3995 (2003).
15. C. Rodríguez and W. Rudolph, "Characterization and $\chi^{(3)}$ measurements of thin films by third-harmonic microscopy," Opt. Lett. **39**(20), 6042–6045 (2014).
16. P. N. Saeta and N. A. Miller, "Distinguishing surface and bulk contributions to third-harmonic generation in silicon," Appl. Phys. Lett. **79**(17), 2704–2706 (2001).
17. D. G. Kong, Q. Chang, H. Ye, Y. C. Gao, Y. X. Wang, X. R. Zhang, K. Yang, W. Z. Wu, and Y. L. Song, "The fifth-order nonlinearity of CS_2," J. Phys. B: At., Mol. Opt. Phys. **42**(6), 065401 (2009).
18. K. Ekvall, C. Lundevall, and P. v. d. Meulen, "Studies of the fifth-order nonlinear susceptibility of ultraviolet-grade fused silica," Opt. Lett. **26**(12), 896–898 (2001).
19. Y.-F. Chen, K. Beckwitt, F. W. Wise, B. G. Aitken, J. S. Sanghera, and I. D. Aggarwal, "Measurement of fifth- and seventh-order nonlinearities of glasses," J. Opt. Soc. Am. B **23**(2), 347–352 (2006).
20. V. Besse, G. Boudebs, and H. Leblond, "Determination of the third- and fifth-order optical nonlinearities: the general case," Appl. Phys. B **116**(4), 911–917 (2014).
21. V. Besse, H. Leblond, and G. Boudebs, "Fifth-order nonlinear susceptibility: Effect of third-order resonances in a classical theory," Phys. Rev. A **92**(1), 013818 (2015).
22. C. Brée, A. Demircan, and G. Steinmeyer, "Saturation of the All-Optical Kerr Effect," Phys. Rev. Lett. **106**(18), 183902 (2011).
23. C. Brée, A. Demircan, and G. Steinmeyer, "Kramers-Kronig relations and high-order nonlinear susceptibilities," Phys. Rev. A **85**(3), 033806 (2012).
24. R. Boyd, *Nonlinear Optics - Third Edition* (Academic Press, 2008).
25. S. Han, L. Ortmann, H. Kim, Y. W. Kim, T. Oka, A. Chacon, B. Doran, M. Ciappina, M. Lewenstein, S.-W. Kim, S. Kim, and A. S. Landsman, "Extraction of higher-order nonlinear electronic response in solids using high harmonic generation," Nat. Commun. **10**(1), 3272 (2019).
26. R. Henking, D. Ristau, F. v. Alvensleben, and H. Welling, "Optical characteristics and damage thresholds of low loss mirrors," in *Laser-Induced Damage in Optical Materials: 1994*, vol. 2428 (SPIE, 1995), pp. 281–292.
27. M. Mende, L. O. Jensen, H. Ehlers, S. Bruns, M. Vergöhl, P. Burdack, and D. Ristau, "Applying hafnia mixtures to enhance the laser-induced damage threshold of coatings for third-harmonic generation optics," in *Laser-Induced Damage in Optical Materials: 2012*, vol. 8530 (International Society for Optics and Photonics, 2012), p. 85300W.
28. ISO, "Optics and photonics — measurement of reflectance of plane surfaces and transmittance of plane parallel elements," Standard, ISO 15368:2021 (2021).
29. M. Sreemany and S. Sen, "A simple spectrophotometric method for determination of the optical constants and band gap energy of multiple layer TiO_2 thin films," Mater. Chem. Phys. **83**(1), 169–177 (2004).
30. S. Rausch, T. Binhammer, A. Harth, J. Kim, R. Ell, F. X. Kärtner, and U. Morgner, "Controlled waveforms on the single-cycle scale from a femtosecond oscillator," Opt. Express **16**(13), 9739–9745 (2008).

31. T. Binhammer, O. Puncken, S. Rausch, B. Schulz, M. Frede, and U. Morgner, "CPA-Free High Repetition Rate Few-Cycle OPCPA," in *2019 Conference on Lasers and Electro-Optics Europe & European Quantum Electronics Conference (CLEO/Europe-EQEC)*, (IEEE, Munich, Germany, 2019), p. 1.

32. K. Yee, "Numerical solution of initial boundary value problems involving maxwell's equations in isotropic media," IEEE Trans. Antennas Propag. **14**(3), 302–307 (1966).

33. "Ansys lumerical FDTD," https://www.ansys.com/products/photonics/fdtd/ (2023).

34. E. D. Palik, *Handbook of optical constants of solids*, vol. 3 (Academic press, 1998).

35. M. F. Al-Kuhaili, "Optical properties of hafnium oxide thin films and their application in energy-efficient windows," Opt. Mater. **27**(3), 383–387 (2004).

36. U. Gubler and C. Bosshard, "Optical third-harmonic generation of fused silica in gas atmosphere: Absolute value of the third-order nonlinear optical susceptibility $\chi^{(3)}$," Phys. Rev. B **61**(16), 10702–10710 (2000).

37. A. Penzkofer, M. Wittmann, M. Lorenz, E. Siegert, and S. Macnamara, "Kerr lens effects in a folded-cavity four-mirror linear resonator," Opt. Quantum Electron. **28**(4), 423–442 (1996).

38. P. Kabacinski, T. M. Kardas, Y. Stepanenko, and C. Radzewicz, "Nonlinear refractive index measurement by SPM-induced phase regression," Opt. Express **27**(8), 11018–11028 (2019).

39. N. Minkovski, G. I. Petrov, S. M. Saltiel, O. Albert, and J. Etchepare, "Nonlinear polarization rotation and orthogonal polarization generation experienced in a single-beam configuration," J. Opt. Soc. Am. B **21**(9), 1659–1664 (2004).

40. L. Gao and Z.-Y. Li, "Temperature Dependence of Nonlinear Optical Properties in Metal/Dielectric Composites," Phys. Status Solidi B **218**(2), 571–582 (2000).